



Modeling of deformation induced anisotropy in free-end torsion

Thomas Böhlke^{a,*}, Albrecht Bertram^a, Erhard Krempl^b

^a*Otto-von-Guericke-University of Magdeburg, Institute of Mechanics, Postfach 4120,
39016 Magdeburg, Germany*

^b*Rensselaer Polytechnic Institute, Mechanics of Materials Laboratory, Troy,
New York 12180, USA*

Received in revised form 16 February 2003

Abstract

The main purpose of this work is to develop a phenomenological model, which accounts for the evolution of the elastic and plastic properties of fcc polycrystals due to a crystallographic texture development and predicts the axial effects in torsion experiments. The anisotropic portion of the effective elasticity tensor is modeled by a growth law. The flow rule depends on the anisotropic part of the elasticity tensor. The normalized anisotropic part of the effective elasticity tensor is equal to the 4th-order coefficient of a tensorial Fourier expansion of the crystal orientation distribution function. Hence, the evolution of elastic and viscoplastic properties is modeled by an evolution equation for the 4th-order moment tensor of the orientation distribution function of an aggregate of cubic crystals. It is shown that the model is able to predict the plastic anisotropy that leads to the monotonic and cyclic Swift effect. The predictions are compared to those of the Taylor–Lin polycrystal model and to experimental data. In contrast to other phenomenological models proposed in the literature, the present model predicts the axial effects even if the initial state of the material is isotropic.

© 2003 Elsevier Ltd. All rights reserved.

Keywords: Anisotropic material; Constitutive behaviour; Finite strain; inhomogeneous material; Polycrystalline material

1. Introduction

If polycrystals consisting of cubic single crystals are subjected to finite, monotonic free-end torsion, an axial strain of about one hundredth the shear strain evolves.

* Corresponding author.

E-mail address: boehlke@mb.uni-magdeburg.de (T. Böhlke).

The effect was first described by Swift (1947), who assumed that hardening mechanisms are responsible for the axial effects. It is now called the Swift effect. If the direction of shear is reversed, then the shear-strain vs. axial-strain curves form a cusp and reach a minimum before axial growth occurs again. This phenomenon is called cyclic Swift effect. A fixed-end torsion results in a development of axial forces.

Swift (1947) performed his experiments to check whether straight radial lines remain straight. The observations on mild steel showed a change of the external dimensions under plastic torsion, which was not in accordance with any known plasticity theory. Therefore, similar tests were performed with 70–30 brass, stainless steel, aluminum, 0.5% carbon steel, copper, and cupro-nickel and different specimen geometries. All materials and all specimen geometries tended to elongate under severe torsional strain. The elongation was therefore not confined to solid circular specimens. Furthermore, the extension effect was found not to be reversible upon reversal of shear. Only a transient tendency to reverse the axial strain was found. This tendency is soon overcome and the tensile straining is re-established. The axial strain accumulation is not dependent on the direction of torsion. Swift also investigated the influence of prior strain and heat treatment. Similar results have been obtained by Stüwe and Turck (1964) and Gil-Sevillano et al. (1975). Swift assumed that the strain hardening causes the axial effects. Billington (1976) contradicted this assumption by experiments. He observed continuous elongations in iron independent of hardening. Nowadays, it has been accepted that the axial effects are due to the crystallographic texture (Montheillet et al., 1985; Harren et al., 1989).

Axial effects are more complex at elevated temperatures. Montheillet et al. (1984) tested polycrystalline samples of Al, Cu, and α -Fe in fixed-end torsion over the temperature range 20–400, 500, and 800 °C. At low temperatures the axial forces were compressive in all three metals. At high temperature the axial forces either changed to small compressive (Al) or to tensile loading (Cu and α -Fe).

Simulations of the torsional deformation provide a suitable means for assessing the adequacy of phenomenological constitutive models. Here the main problem of a constitutive model is the representing of the axial deformation behavior in a cyclic torsion test at large shear strains. Montheillet et al. (1985) have shown that, if the ellipsoidal yield surface, proposed by von Mises (1928) and Hill (1948), is specified by the ideal orientations found in torsion textures, then the monotonic Swift effect can be reproduced. But there is no evolution equation given that describes the evolving anisotropy. Harren et al. (1989) simulated Swift's reverse torsion test using a rate-dependent Taylor type polycrystal model. In this simulation, performed with 500 single crystals, the cyclic Swift effect has been reproduced. The magnitude of the axial strains is overestimated by the Taylor type model by approximately a factor of three. Van der Giessen et al. (1992) considered two different phenomenological models for the plastic spin. The influence on the predicted torque response and the axial strain effects in a large strain torsion of a solid circular bar was investigated. It is found that the differences in the predicted axial effects are more pronounced in the fixed-end case whereas the differences in the torque response is more pronounced in

the free-end case. In the free-end case the simulation shows a monotonically increasing lengthening. Van der Giessen et al. (1992) do not investigate a cyclic torsion test. Other approaches considering the monotonic Swift effect or torsional deformations are given by Pan (1996, 1997); Wu et al. (1997); Ishikawa (1999); Xiao et al. (2001); Barlat et al. (2002); Wu (2003). The coupling between texture and macroscopic material response is studied by Cho and Dafalias (1996); Miller and McDowell (1996); Man (2002).

Hahne (1993) provides a complete review of papers on the Swift effect. Furthermore, Hahne models the cyclic Swift effect macroscopically. He postulates a quadratic yield condition in terms of the stress deviator. The evolution equation of the 4th-order tensor, which occurs in the quadratic form, is specified by a corotational rate. The rate of change of the 4th-order tensor is assumed to be proportional to the dyadic product of the stress deviator. The identification of the material parameters requires the application of an optimization procedure.

Majors and Krempl (1994) discussed two classes of phenomenological models qualitatively. The first class is given by models based on a 2nd-order backstress tensor. The plastic flow is assumed to have the same direction as the difference of the Cauchy stress and the backstress. In contrast to experiments, the model predicts that the axial growth continues immediately after reversal. The second class is given by models in which the plastic rate of deformation is given as a (generally anisotropic) map of the difference of the Cauchy stress and the backstress. It is found that both classes are able to reproduce the monotonic Swift effect. It is furthermore shown that the first class is not able to model the cyclic Swift effect (see also, Portier et al., 2000).

Kuroda (1997) developed a phenomenological viscoplastic model in order to describe the cyclic Swift effect. An orthotropic yield surface is introduced. The orthotropic axes are assumed to rotate with the elastic portion of the spin tensor. This elastic portion is given by the difference of the spin tensor and the Eulerian form of the plastic spin. The plastic spin is modeled by the assumption that it is driven by the non-coaxiality of the stress tensor and the inelastic rate of deformation. The cyclic Swift effect can be reproduced by this approach. The strain hardening is found to be of minor importance. Kuroda (1999) compared the predictions of the aforementioned phenomenological model with Taylor type simulations. He showed that both models predict similar yield loci and reproduce the cyclic Swift effect, but overestimate the axial strains. In Kuroda's model only the directions of the orthotropic axes are changed by inelastic deformations. The parameters with respect to the orthotropic axes are constant. This implies that the material must already be anisotropic in the initial state in order to make the approach successful. Hence this approach is of limited applicability.

1.1. Outline of the paper

In Section 2 we introduce two models for the description of polycrystals: a phenomenological model and a polycrystal model. The phenomenological model has been discussed in detail by Böhlke and Bertram (2001) for the special case of

deformations which can be described by a symmetric velocity gradient. In the present paper we apply an extension of this model which includes the plastic spin and allows for a modeling of the axial behavior in torsion experiments of fcc polycrystals at room temperature. The phenomenological approach models the growth of the anisotropic part of the effective elasticity tensor. The flow rule depends on the anisotropic part of the elasticity tensor. This type of a coupling is substantiated by experimental and theoretical findings (Stickels and Mould, 1970; Man, 1995). It can be shown, that the normalized anisotropic part of the effective elasticity tensor is equal to a 4th-order coefficient of a tensorial Fourier expansion of the crystal orientation distribution function (Böhlke and Bertram, 2002). Hence, the evolution of elastic and viscoplastic properties is modeled by an evolution equation for the 4th-order moment tensor of the orientation distribution function of an aggregate of cubic crystals. The polycrystal model is the Taylor–Lin model (Taylor, 1938; Lin, 1957; Harren et al., 1989) which has been applied often in the context of texture simulations. In Section 3 the phenomenological model and the polycrystal model are compared with respect to the predictions of axial effects in free-end torsion experiments with polycrystalline copper. Both the monotonic and the cyclic Swift effect are investigated. The phenomenological model reproduces the axial effects. The numerical results are compared with experimental data presented by Swift (1947).

1.2. Notation

Throughout the text a direct tensor notation is preferred. To avoid additional formal definitions, the index notation is applied in some cases using the summation convention. A linear mapping of a 2nd-order tensor is written as $\mathbf{A} = \mathbb{C}[\mathbf{B}]$. The scalar product, the dyadic product, and the Frobenius norm are denoted by $\mathbf{A} \cdot \mathbf{B} = \text{tr}(\mathbf{A}^T \mathbf{B})$, $\mathbf{A} \otimes \mathbf{B}$, and $\|\mathbf{A}\| = (\mathbf{A} \cdot \mathbf{A})^{1/2}$, respectively. $\mathbf{I} = \mathbf{e}_i \otimes \mathbf{e}_i$ and $\mathbb{I} = \mathbf{e}_i \otimes \mathbf{e}_j \otimes (\mathbf{e}_i \otimes \mathbf{e}_j + \mathbf{e}_j \otimes \mathbf{e}_i) / 2$ denote the 2nd-order identity and the identity on symmetric 2nd-order tensors. Irreducible, i.e., completely symmetric and traceless tensors are designated by a prime, e.g., \mathbf{A}' and \mathbb{C}' . The symmetric and the skew-symmetric part of a 2nd-order tensor \mathbf{A} are denoted by $\text{sym}(\mathbf{A})$ and $\text{skw}(\mathbf{A})$, respectively. The Rayleigh product $\mathbf{A} * \mathbb{C}$ of a 4th-order tensor $\mathbb{C} = C_{ijkl} \mathbf{e}_i \otimes \mathbf{e}_j \otimes \mathbf{e}_k \otimes \mathbf{e}_l$ and a 2nd-order tensor $\mathbf{A} = A_{ij} \mathbf{e}_i \otimes \mathbf{e}_j$ is defined by

$$\mathbf{A} * \mathbb{C} = C_{ijkl} (\mathbf{Ae}_i) \otimes (\mathbf{Ae}_j) \otimes (\mathbf{Ae}_k) \otimes (\mathbf{Ae}_l), \quad (1)$$

where $\{\mathbf{e}_i\}$ is an orthonormal basis. If \mathbb{C} exhibits a symmetry in the first or second pair of indices (e.g., $C_{ijkl} = C_{jikl}$) or the major symmetry ($C_{ijkl} = C_{klij}$), $\mathbf{A} * \mathbb{C}$ shows the same symmetry properties for all \mathbf{A} . The associativity $\mathbf{A} * (\mathbf{B} * \mathbb{C}) = (\mathbf{AB}) * \mathbb{C}$ holds for all 2nd-order tensors \mathbf{A} and \mathbf{B} . The bracket formula $\{\cdot\}$ is defined by ($\mathbf{A}, \mathbf{B} \in \text{Sym}$)

$$\{A_{ij} B_{kl}\} = \frac{1}{6} (A_{ij} B_{kl} + A_{ik} B_{jl} + A_{il} B_{kj} + B_{ij} A_{kl} + B_{ik} A_{jl} + B_{il} A_{kj}) \quad (2)$$

2. A phenomenological and a polycrystal model

2.1. The phenomenological model

2.1.1. Elastic law

2.1.1.1. Anisotropic hyperelastic stress–strain relation. The stress–strain relation applied here is equivalent to the standard formulation of the theory of elasto-plasticity based on a linear elastic law of the St. Venant type. The Kirchhoff stress tensor τ_e is given as a linear map of the elastic Almansi strain tensor (e.g., Böhlke and Bertram, 2001)

$$\tau_e = \mathbb{C}_e[\mathbf{E}_e^A], \quad \mathbf{E}_e^A = \frac{1}{2}(\mathbf{I} - \mathbf{F}_e^{-T}\mathbf{F}_e^{-1}), \quad \mathbf{F}_e = \mathbf{F}\mathbf{F}_p^{-1}. \quad (3)$$

The Kirchhoff stress τ_e is defined by the Cauchy stress σ and the determinant J_e of \mathbf{F}_e through $\tau_e = J_e\sigma$. The tensor \mathbf{F}_e represents the elastic portion of the deformation gradient $\mathbf{F} = \mathbf{F}_e\mathbf{F}_p$. The multiplicative decomposition of the deformation gradient into elastic and plastic parts can be derived by the assumption of isomorphic elastic ranges (Bertram, 1992, 1999). In the present work it is assumed that the decomposition holds even if the elastic properties evolve with crystallographic texture (Böhlke, 2001).

The stiffness operator \mathbb{C}_e is given by the Rayleigh product of \mathbf{F}_e and the reference stiffness tensor $\tilde{\mathbb{C}}$

$$\mathbb{C}_e = \mathbf{F}_e * \tilde{\mathbb{C}} = \tilde{C}_{ijkl}(\mathbf{F}_e\mathbf{e}_i) \otimes (\mathbf{F}_e\mathbf{e}_j) \otimes (\mathbf{F}_e\mathbf{e}_k) \otimes (\mathbf{F}_e\mathbf{e}_l). \quad (4)$$

Note, that the tensor \mathbb{C}_e is generally non-constant even in the case that $\tilde{\mathbb{C}}$ is constant and isotropic. Within the standard formulation of the theory of elasto-plasticity, i.e. without induced elastic anisotropy, $\tilde{\mathbb{C}}$ is assumed to be constant. Here and in the subsequent sections a tilde indicates that the quantities are formulated with respect to the undistorted configuration, which is characterized by the fact that corresponding symmetry transformations are elements of the orthogonal group.

2.1.1.2. Decomposition of Hooke's tensor. Volume averages of stiffnesses or compliances with a cubic symmetry generally allow for the following unique decomposition of the effective properties into three different parts, e.g., in terms of stiffnesses

$$\tilde{\mathbb{C}} = 3K\mathbb{P}_1^I + 2G\mathbb{P}_2^I + \zeta\tilde{\mathbb{A}}^I, \quad \mathbb{P}_1^I = \frac{1}{3}\mathbf{I} \otimes \mathbf{I}, \quad \mathbb{P}_2^I = \mathbb{I} - \mathbb{P}_1^I. \quad (5)$$

This result holds for the arithmetic, the harmonic mean, or the geometric mean of stiffness tensors (Böhlke and Bertram, 2000, 2001). The two 4th-order tensors \mathbb{P}_1^I and \mathbb{P}_2^I represent the isotropic part of the elastic law, which is independent of the crystallographic texture in the aggregate. The constants K , G , ζ depend on the type of averaging. K is the bulk modulus and G is the shear modulus. ζ quantities the

amount of anisotropy of the cubic crystals forming the aggregate and also depends on the type of averaging.

2.1.1.3. Micromechanical interpretation of the decomposition. The tensor \mathbb{A}' specifies the direction of the purely anisotropic part of the stiffness tensor $\hat{\mathbb{C}}$. A property which is characteristic for aggregates of cubic crystals is that the anisotropic part \mathbb{A}' is independent of the special type of averaging (Böhlke and Bertram, 2001). It is given in terms of a mean value

$$\tilde{\mathbb{A}}' = \frac{\sqrt{30}}{30} \left(\mathbf{I} \otimes \mathbf{I} + 2\mathbb{1} - 5 \int_g f(g) \sum_{i=1}^3 \tilde{\mathbf{g}}_i(g) \otimes \tilde{\mathbf{g}}_i(g) \otimes \tilde{\mathbf{g}}_i(g) \otimes \tilde{\mathbf{g}}_i(g) dg \right), \quad (6)$$

where $\{\tilde{\mathbf{g}}_i\}$ denotes the lattice vectors of the single crystals on the microscale. $f(g)$ represents the crystal orientation distribution function. The function f specifies the volume fraction of crystals having an orientation between g and $g + dg$, i.e. $dV/V = f(g)dg$. If there is no crystallographic texture in the aggregate, then $\tilde{\mathbb{A}}' = 0$ holds and $\hat{\mathbb{C}}$ is isotropic. By definition the Frobenius norm of $\tilde{\mathbb{A}}'$ is equal to one for a single crystal orientation. The tensor $\tilde{\mathbb{A}}'$ is symmetric and traceless with respect to all pairs of indices

$$\tilde{A}'_{ijkl} = \tilde{A}'_{jikl} = \tilde{A}'_{klij} = \tilde{A}'_{kjil} = \dots, \quad \tilde{A}'_{iikl} = 0. \quad (7)$$

As a result, $\tilde{\mathbb{A}}'$ contains only nine independent components, and this property leads to a rigorous simplification of the evolution equation of $\tilde{\mathbb{A}}'$. The tensor $\tilde{\mathbb{A}}'$ represents the 4th-order coefficient of a tensorial Fourier expansion of the crystal orientation distribution function of an aggregate of cubic crystals (Böhlke and Bertram, 2002).

2.1.2. Flow rule

2.1.2.1. The coupling of elastic and plastic anisotropy. There is experimental evidence that for textured polycrystals the effective elastic and (visco)plastic properties are correlated (Bunge and Roberts, 1969; Stickels and Mould, 1970; Kallend and Davies, 1971; Davies et al., 1972). Therefore, the anisotropy of the (visco)plastic behavior can be inferred not only from destructive tests but also from non-destructive measurements of the elastic anisotropy parameters. Based on these findings, Man (1995, 1998) formulated a quadratic yield function which assumes that the elastic and plastic properties are correlated linearly. As a result, the anisotropic part of the effective elasticity tensors specifies the anisotropic part of the quadratic yield condition. The introduction of a quadratic yield function goes back to von Mises (1928) who used a general 4th-order tensor to formulate a quadratic yield condition in terms of stresses.

2.1.2.2. Flow rule. In the following it is convenient to decompose the flow rule into its symmetric $\tilde{\mathbf{D}}_p$ and skew part $\tilde{\mathbf{W}}_p$

$$\dot{\mathbf{F}}_p \mathbf{F}_p^{-1} = \tilde{\mathbf{D}}_p + \tilde{\mathbf{W}}_p. \quad (8)$$

The directions of $\tilde{\mathbf{D}}_p$ and $\tilde{\mathbf{W}}_p$ are denoted by $\tilde{\mathbf{N}}_p = \tilde{\mathbf{D}}_p / \|\tilde{\mathbf{D}}_p\|$ and $\tilde{\mathbf{M}}_p = \tilde{\mathbf{W}}_p / \|\tilde{\mathbf{W}}_p\|$, respectively. The viscoplastic flow is assumed to be driven by an overstress. The direction of $\tilde{\mathbf{D}}_p$ is specified by the stress tensor and the anisotropic portion of the effective elasticity tensor

$$\tilde{\mathbf{D}}_p = \frac{\dot{\gamma}_0}{\|\tilde{\mathbf{S}}'\|} \left\langle \frac{\sqrt{\frac{3}{2}} \|\tilde{\mathbf{S}}'\|_a - \sigma_F}{\sigma_D} \right\rangle^{\frac{1}{m}} \tilde{\mathbb{N}}(\eta, \tilde{\mathbb{A}}') [\tilde{\mathbf{S}}'], \quad \tilde{\mathbb{N}}(\eta, \tilde{\mathbb{A}}') = \mathbb{P}_2^I + \eta \tilde{\mathbb{A}}'. \tag{9}$$

The bracket $\langle x \rangle$ is defined by $(x + |x|)/2$. The flow rule is rate-dependent and this rate-dependence is specified by the scalar m . The scalars σ_F and σ_D represent a critical flow stress and a drag stress, respectively. The scalar $\dot{\gamma}_0$ is a referential inelastic rate. With $\|\tilde{\mathbf{S}}'\|_a$ we denote an anisotropic norm of the deviator $\tilde{\mathbf{S}}'$

$$\|\tilde{\mathbf{S}}'\|_a = \sqrt{\tilde{\mathbf{S}}' \cdot \tilde{\mathbb{N}}(\eta, \tilde{\mathbb{A}}') [\tilde{\mathbf{S}}']}, \quad \tilde{\mathbf{S}} = \mathbf{F}_e^{-1} \boldsymbol{\tau}_e \mathbf{F}_e^{-T}. \tag{10}$$

The anisotropic part of the norm is governed by the scalar η and the tensor $\tilde{\mathbb{A}}'$. Keeping in mind that \mathbb{P}_2^I is the identity on symmetric and traceless 2nd-order tensors, then it is not hard to see, that for the elastically isotropic case a rate-dependent J_2 -theory is obtained.

The constitutive relation for the non-symmetric part of the flow rule, i.e. the plastic spin, is formulated close to a suggestion by Kuroda (1997) (see also Kuroda, 1999) which is based on papers by Zbib and Aifantis (1988) and Zbib (1991). The plastic spin $\tilde{\mathbf{W}}_p$ is assumed to be proportional to the noncoaxiality of the stress and the inelastic rate of deformation

$$\tilde{\mathbf{W}}_p = \dot{\gamma}_0 \left\langle \frac{\sqrt{\frac{3}{2}} \|\tilde{\mathbf{S}}'\|_a - \sigma_F}{\sigma_D} \right\rangle^{\frac{1}{m}} \frac{\tilde{\mathbf{S}}' \tilde{\mathbf{D}}'_p - \tilde{\mathbf{D}}'_p \tilde{\mathbf{S}}'}{\|\tilde{\mathbf{S}}' \tilde{\mathbf{D}}'_p - \tilde{\mathbf{D}}'_p \tilde{\mathbf{S}}'\|}. \tag{11}$$

2.1.3. Growth law for the elasticity tensor

2.1.3.1. *Symmetric velocity gradients.* For the modeling of the evolution of $\tilde{\mathbb{A}}'$ for deformations which can be described by symmetric velocity gradients the following ansatz has been applied by Böhlke (2001) and Böhlke and Bertram (2001)

$$\dot{\tilde{\mathbb{A}}}' = \|\tilde{\mathbf{D}}'_p\| \left(\tilde{\mathbb{G}}'(\tilde{\mathbf{N}}'_p) - d(I_{p1}) \tilde{\mathbb{A}}' \right), \quad I_{p1} = \det(\tilde{\mathbf{N}}'_p). \tag{12}$$

This ansatz is formally similar to kinematic hardening models based on 2nd-order tensors (see, e.g., Armstrong and Frederick, 1966). Krempl (1994) proposed such type of an evolution equation for a 4th-order plastic compliance tensor. The growth law for $\tilde{\mathbb{A}}'$ has to be isotropic since the anisotropy is taken explicitly into account by the tensor $\tilde{\mathbb{A}}'$. The driving term $\tilde{\mathbb{G}}'(\tilde{\mathbf{N}}'_p)$ depends only on the direction $\tilde{\mathbf{N}}'_p$ of the inelastic rate of deformation $\tilde{\mathbf{D}}'_p$ which is the symmetric part of $\dot{\mathbf{F}}_p \mathbf{F}_p^{-1}$. The ansatz (12) takes into account that for constant strain rates the crystallographic texture tends to saturate for large deformations. The saturation behavior is controlled by

$d(I_{p1}) \tilde{\mathbb{A}}'$. The function $d(I_{p1})$ depends on the only non-constant principal invariant of $\tilde{\mathbf{N}}'_p$, i.e., its determinant.

Due to the constraint that, similar to $\tilde{\mathbb{A}}'$, the function $\tilde{\mathbb{G}}'$ has to be symmetric and traceless with respect to all pairs of indices, the function $\tilde{\mathbb{G}}'$ is generally given by three 4th-order tensor generators $\tilde{\mathbb{G}}'_\alpha$ and corresponding scalar functions G_α (Böhlke and Bertram, 2001)

$$\tilde{\mathbb{G}}'(\tilde{\mathbf{N}}'_p) = G_1(I_{p1})\tilde{\mathbb{G}}'_1(\tilde{\mathbf{N}}'_p) + G_2(I_{p1})\tilde{\mathbb{G}}'_2(\tilde{\mathbf{N}}'_p) + G_3(I_{p1})\tilde{\mathbb{G}}'_3(\tilde{\mathbf{N}}'_p). \tag{13}$$

The tensor generators are

$$\begin{aligned} \mathbb{G}_1(\mathbf{N}') &= \{\mathbf{N}' \otimes \mathbf{N}'\} - \frac{4}{7}\{\mathbf{N}'^2 \otimes \mathbf{I}\} + \frac{2}{35}\text{tr}(\mathbf{N}'^2)\{\mathbf{I} \otimes \mathbf{I}\}, \\ \mathbb{G}_2(\mathbf{N}') &= \{\mathbf{N}'^2 \otimes \mathbf{N}'^2\} - \frac{2}{7}\left(\text{tr}(\mathbf{N}'^2)\{\mathbf{N}'^2 \otimes \mathbf{I}\} \right. \\ &\quad \left. + 2\{\mathbf{N}'^4 \otimes \mathbf{I}\}\right) + \frac{1}{35}\left(\text{tr}(\mathbf{N}'^2)^2 + 2\text{tr}(\mathbf{N}'^4)\right)\{\mathbf{I} \otimes \mathbf{I}\}, \\ \mathbb{G}_3(\mathbf{N}') &= \{\mathbf{N}'^2 \otimes \mathbf{N}'\} - \frac{2}{7}\left(\text{tr}(\mathbf{N}'^2)\{\mathbf{N}'^2 \otimes \mathbf{I}\} + 4\{\mathbf{N}'^3 \otimes \mathbf{I}\}\right) \\ &\quad + \frac{4}{35}\text{tr}(\mathbf{N}'^3)\{\mathbf{I} \otimes \mathbf{I}\}. \end{aligned} \tag{14}$$

In Table 1 the material functions are summarized.

Table 1
Material functions on the macroscale (symmetric velocity gradients)

Elastic law	$\boldsymbol{\tau}_e = \mathbb{C}_e[\mathbf{E}_e^A] \quad \mathbb{C}_e = \mathbf{F}_e * \tilde{\mathbb{C}}$	(3)
Stiffness tensor	$\tilde{\mathbb{C}} = 3K\mathbb{P}_1^I + 2G\mathbb{P}_2^I + \zeta\tilde{\mathbb{A}}'$	(5)
Interpretation	$\tilde{\mathbb{A}}' = \frac{\sqrt{30}}{30}\left(\mathbf{I} \otimes \mathbf{I} + 2\mathbb{I} - 5 \int_g f(g) \sum_{i=1}^3 \tilde{\mathbf{g}}_i(g) \otimes \tilde{\mathbf{g}}_i(g) \otimes \tilde{\mathbf{g}}_i(g) \otimes \tilde{\mathbf{g}}_i(g) dg\right)$	(6)
Properties	$\tilde{A}'_{ijkl} = \tilde{A}'_{jikl} = \tilde{A}'_{klij} = \tilde{A}'_{kji l} = \dots, \quad \tilde{A}'_{iikl} = 0$	(7)
Flow rule	$\tilde{\mathbf{D}}_p = \text{sym}(\dot{\mathbf{F}}_p \mathbf{F}_p^{-1}) = \frac{\dot{\gamma}_0}{\ \tilde{\mathbf{S}}'\ _a} \left\langle \frac{\sqrt{\frac{3}{2}} \ \tilde{\mathbf{S}}'\ _a - \sigma_F}{\sigma_D} \right\rangle^{\frac{1}{m}} \tilde{\mathbb{N}}[\tilde{\mathbf{S}}']$ $\tilde{\mathbf{W}}_p = \text{skw}(\dot{\mathbf{F}}_p \mathbf{F}_p^{-1}) = 0$	(9)
Inelastic compliance	$\tilde{\mathbb{N}} = \tilde{\mathbb{P}}_2^I + \eta\tilde{\mathbb{A}}'$	(9)
Anisotropic norm	$\ \tilde{\mathbf{S}}'\ _a = \sqrt{\tilde{\mathbf{S}}' \cdot \tilde{\mathbb{N}}[\tilde{\mathbf{S}}']}$	(10)
Growth law	$\dot{\tilde{\mathbb{A}}}' = \ \tilde{\mathbf{D}}'_p\ \left(\tilde{\mathbb{G}}'(\tilde{\mathbf{N}}'_p) - d(I_{p1})\tilde{\mathbb{A}}' \right)$ $\tilde{\mathbf{N}}'_p = \tilde{\mathbf{D}}'_p / \ \tilde{\mathbf{D}}'_p\ \quad I_{p1} = \det(\tilde{\mathbf{N}}'_p)$	(12)
Tensor valued function	$\mathbb{G}'(\tilde{\mathbf{N}}'_p) = G_1(I_{p1})\mathbb{G}'_1(\tilde{\mathbf{N}}'_p) + G_2(I_{p1})\mathbb{G}'_2(\tilde{\mathbf{N}}'_p) + G_3(I_{p1})\mathbb{G}'_3(\tilde{\mathbf{N}}'_p)$	(13)

2.1.3.2. *Non-symmetric velocity gradients.* In order to describe deformations which have to be described by non-symmetric and non-skew velocity gradients, Eq. (12) has to be extended to include the plastic spin. A simple extension of the ansatz (12) is given by

$$\dot{\tilde{\mathbb{A}}}' = \|\dot{\tilde{\mathbf{F}}}_p \mathbf{F}_p^{-1}\| \left(\tilde{\mathbb{G}}'(\tilde{\mathbf{N}}'_p, \tilde{\mathbf{M}}'_p) - d(\tilde{\mathbf{N}}'_p, \tilde{\mathbf{M}}'_p) \tilde{\mathbb{A}}' \right). \quad (15)$$

In contrast to (12) the driving term $\tilde{\mathbb{G}}'(\tilde{\mathbf{N}}'_p, \tilde{\mathbf{M}}'_p)$ depends on the directions $\tilde{\mathbf{N}}'_p$ of $\tilde{\mathbf{D}}'_p$ and $\tilde{\mathbf{M}}'_p$ of $\tilde{\mathbf{W}}_p$. Furthermore, the function d , which governs the saturation behavior, is a function of $\tilde{\mathbf{N}}'_p$ and $\tilde{\mathbf{M}}'_p$. The 4th-order tensor function $\tilde{\mathbb{G}}'(\tilde{\mathbf{N}}'_p, \tilde{\mathbf{M}}'_p)$ and the scalar function $d(\tilde{\mathbf{N}}'_p, \tilde{\mathbf{M}}'_p)$ can be determined by means of the theory of isotropic tensor functions. The general representation of the tensor function \mathbb{G}' has been given by Böhlke (2001). The function \mathbb{G}' depends on three tensor generators which depend only on $\tilde{\mathbf{N}}'_p$, on one tensor generator, which depends only on $\tilde{\mathbf{M}}'_p$, and 23 generators, which depend simultaneously on $\tilde{\mathbf{N}}'_p$ and $\tilde{\mathbf{M}}'_p$.

It can be shown that the induced anisotropy caused by shear deformations can be described using tensor generators which depend only on $\tilde{\mathbf{D}}_p$ or $\tilde{\mathbf{W}}_p$ but not simultaneously on $\tilde{\mathbf{D}}_p$ and $\tilde{\mathbf{W}}_p$ (Böhlke, 2001). The tensor generator depending only on $\tilde{\mathbf{W}}_p$ is given by $\mathbb{G}'_2(\tilde{\mathbf{M}}_p)$. Hence a simple extension of the evolution Eq. (12) is given by

$$\begin{aligned} \dot{\tilde{\mathbb{A}}}' = \|\dot{\tilde{\mathbf{F}}}_p \mathbf{F}_p^{-1}\| & \left(G_1(I_{p1}) \mathbb{G}'_1(\tilde{\mathbf{N}}'_p) + G_2(I_{p1}) \mathbb{G}'_2(\tilde{\mathbf{N}}'_p) + G_3(I_{p1}) \mathbb{G}'_3(\tilde{\mathbf{N}}'_p) \right. \\ & \left. + G_4(I_{p2}) \mathbb{G}'_2(\tilde{\mathbf{M}}'_p) - d(\tilde{\mathbf{N}}'_p, \tilde{\mathbf{M}}'_p) \tilde{\mathbb{A}}' \right) \end{aligned} \quad (16)$$

Note that I_{p1} and $I_{p2} = \text{tr}(\tilde{\mathbf{M}}_p^2)$ are the only non-constant invariants of $\tilde{\mathbf{N}}_p$ and $\tilde{\mathbf{M}}_p$, respectively. In Table 2 the modified set of material functions is given. The identification of the material functions and parameters is discussed in detail by Böhlke (2001). There it is shown that texture simulations indicate constraints between the functions G_i (see, Tables 3 and 4). In Table 5 all material parameters are summarized.

If the elastic anisotropy of the single crystals is small, e.g. in the case of Aluminum, the same phenomenological model can be applied as suggested in the preceding sections. Note that in the case of aluminum, the scalar factor ζ is much smaller than for copper. Hence the anisotropic part of the effective stiffness may be neglected. But nevertheless the texture evolution is taken into account by modeling the anisotropy of the flow rule in terms of the tensor \mathbb{A}' .

2.2. The Taylor–Lin polycrystal model

2.2.1. Micro–macro transition

In contrast to Taylor's (1938) original rigid-plastic approach here the Taylor–Lin model (Lin, 1957) is applied, which allows for elastic deformations of the crystal lattices. Similar to the Taylor approach the Taylor–Lin model treats compatibility constraints as paramount. Hence, the aggregate is assumed to deform homogeneously. The equilibrium conditions are violated on the grain boundaries. The

Table 2
Material functions on the macroscale (non-symmetric velocity gradients)

Flow rule	$\tilde{\mathbf{D}}_p = \text{sym}(\dot{\mathbf{F}}_p \mathbf{F}_p^{-1}) = \frac{\dot{\gamma}_0}{\ \tilde{\mathbf{S}}'\ _a} \left\langle \frac{\sqrt{\frac{3}{2}} \ \tilde{\mathbf{S}}'\ _a - \sigma_F}{\sigma_D} \right\rangle^{\frac{1}{m}} \tilde{\mathbb{N}}[\tilde{\mathbf{S}}']$	(9)
	$\tilde{\mathbf{W}}_p = \text{skw}(\dot{\mathbf{F}}_p \mathbf{F}_p^{-1}) = \dot{\gamma}_0 \left\langle \frac{\sqrt{\frac{3}{2}} \ \tilde{\mathbf{S}}'\ _a - \sigma_F}{\sigma_D} \right\rangle^{\frac{1}{m}} \frac{\tilde{\mathbf{S}}' \tilde{\mathbf{D}}'_p - \tilde{\mathbf{D}}'_p \tilde{\mathbf{S}}'}{\ \tilde{\mathbf{S}}' \tilde{\mathbf{D}}'_p - \tilde{\mathbf{D}}'_p \tilde{\mathbf{S}}'\ }$	(11)
Inelastic compliance	$\tilde{\mathbb{N}} = \tilde{\mathbb{P}}_2' + \eta \tilde{\mathbb{A}}'$	(9)
Anisotropic norm	$\ \tilde{\mathbf{S}}'\ _a = \sqrt{\tilde{\mathbf{S}}' \cdot \tilde{\mathbb{N}}[\tilde{\mathbf{S}}']}$	(10)
Growth law	$\dot{\tilde{\mathbb{A}}}' = \ \tilde{\mathbf{D}}'_p\ \left(\mathbb{G}'(\tilde{\mathbf{N}}'_p, \tilde{\mathbf{M}}_p) - d(\tilde{\mathbf{N}}'_p, \tilde{\mathbf{M}}_p) \tilde{\mathbb{A}}' \right)$	(16)
	$\tilde{\mathbf{N}}'_p = \tilde{\mathbf{D}}'_p / \ \tilde{\mathbf{D}}'_p\ \quad I_{p1} = \det(\tilde{\mathbf{N}}'_p) \quad \tilde{\mathbf{M}}_p = \tilde{\mathbf{W}}_p / \ \tilde{\mathbf{W}}_p\ \quad I_{p2} = \text{tr}(\tilde{\mathbf{M}}_p^2)$	
Tensor valued function	$\mathbb{G}'(\tilde{\mathbf{N}}'_p) = G_1(I_{p1}) \mathbb{G}'_1(\tilde{\mathbf{N}}'_p) + G_2(I_{p1}) \mathbb{G}'_2(\tilde{\mathbf{N}}'_p) + G_3(I_{p1}) \mathbb{G}'_3(\tilde{\mathbf{N}}'_p) + G_4(I_{p2}) \mathbb{G}'_2(\tilde{\mathbf{M}}_p)$	(16)

Table 3
Material functions on the macroscale I

$G_1(I_{p1})$	$G_2(I_{p1})$	$G_3(I_{p1})$	$G_4(I_{p1})$
$\frac{\sqrt{2}}{14} \left(1 + \frac{497\sqrt{6}}{66} I_{p1} \right) G(I_{p1})$	$\frac{17\sqrt{2}}{7} G(I_{p1})$	$\left(1 - \frac{629\sqrt{3}}{483} - 4 \right) \frac{3\sqrt{6}}{2} G(I_{p1})$	-1.5

Table 4
Material functions on the macroscale II ($\xi \approx -3\sqrt{6}I_{p1}/2$)

	$\xi = -0.50$	$\xi = -0.25$	$\xi = 0.0$	$\xi = 0.25$	$\xi = 0.50$
$G(I_{p1})$	0.25	0.50	0.38	0.26	2.50
$d(I_{p1})$	2.35	2.05	0.44	0.04	2.00

Table 5
Material parameters on the macroscale

K	G	ζ	σ_D	$\dot{\gamma}_0$	m	η	d
136.93 GPa	54.56 GPa	114.14 GPa	46.5 MPa	0.001 s ⁻¹	0.0125	0.9	0.44

simulations discussed in the present work have been performed with 1000 different crystal orientations. The initial orientations are filtered random orientations (Böhlke and Bertram, 1998). Between every pair of initial orientations there is a minimum distance of $d^G = 1.5^\circ$ guaranteed. The deformation is prescribed in terms of a velocity gradient.

2.2.2. Elastic law

In contrast to the macroscale the reference stiffness $\tilde{\mathbb{C}}$ is constant on the microscale. In the case of a cubic symmetry, the elasticity tensors have three distinct eigenvalues. The stiffness tensor can be written in terms of eigenvalues and corresponding eigenprojections (e.g., Böhlke and Bertram, 2001)

$$\tilde{\mathbb{C}} = \sum_{\alpha=1}^3 \lambda_\alpha \mathbb{P}_\alpha^C. \tag{17}$$

The projectors \mathbb{P}_α^C are idempotent $\mathbb{P}_\alpha^C \mathbb{P}_\alpha^C = \mathbb{P}_\alpha^C$, biorthogonal $\mathbb{P}_\alpha^C \mathbb{P}_\beta^C = \mathbb{0} (\alpha \neq \beta)$, and complete $\sum_{\alpha=1}^3 \mathbb{P}_\alpha^C = \mathbb{I}$. The cubic projectors are

$$\mathbb{P}_1^C = \mathbb{P}^I, \quad \mathbb{P}_2^C = \mathbb{D} - \mathbb{P}_1^C, \quad \mathbb{P}_3^C = \mathbb{I} - \mathbb{P}_2^C - \mathbb{P}_1^C. \tag{18}$$

The anisotropic part \mathbb{D} is given by a dyadic product of lattice vectors $\tilde{\mathbf{g}}_i$

$$\mathbb{D} = \sum_{i=1}^3 \tilde{\mathbf{g}}_i \otimes \tilde{\mathbf{g}}_i \otimes \tilde{\mathbf{g}}_i \otimes \tilde{\mathbf{g}}_i. \tag{19}$$

The eigenvalues λ_α can be written in terms of the components of \mathbb{C} with respect to the orthonormal lattice vectors $\{\mathbf{g}_i\}$ ($i = 1, 2, 3$): $\lambda_1 = C_{1111} + 2C_{1122}$, $\lambda_2 = C_{1111} - C_{1122}$, and $\lambda_3 = 2C_{1212}$.

2.2.3. Flow rule

Inelastic deformations in single crystals at room temperature are dominated by slip mechanisms on specific crystallographic planes. For the description of copper, a slip system theory with the twelve octahedral slip systems is applicable. The flow rule is specified by slip directions $\tilde{\mathbf{d}}_\alpha$, slip plane normals $\tilde{\mathbf{n}}^\alpha$, and corresponding slip system shear rates $\dot{\gamma}_\alpha$

$$\dot{\mathbf{F}}_p \mathbf{F}_p^{-1} = \sum_{\alpha=1}^{12} \dot{\gamma}_\alpha \tilde{\mathbf{d}}_\alpha \otimes \tilde{\mathbf{n}}^\alpha, \quad \dot{\gamma}_\alpha = \dot{\gamma}_\alpha(\tau_\alpha, z_\alpha), \quad \tau_\alpha = \tilde{\mathbb{C}} \tilde{\mathbf{S}} \cdot \tilde{\mathbf{d}}_\alpha \otimes \tilde{\mathbf{n}}^\alpha. \tag{20}$$

$\tilde{\mathbb{C}} = \tilde{\mathbf{F}}^T \tilde{\mathbb{F}}$ denotes the right Cauchy-Green tensor with respect to $\tilde{\mathbf{F}}$. A viscoplastic relation for the $\dot{\gamma}_\alpha$ is applied in the present paper

$$\dot{\gamma}_0 = \dot{\gamma}_0 \text{sign}(\tau_\alpha) \left\langle \frac{|\tau_\alpha| - \tau_\alpha^C}{\tau_\alpha^D} \right\rangle^{\frac{1}{m}} \tag{21}$$

(Méric and Cailletaud, 1992; Méric et al., 1994). The variable τ_α^C is a critical resolved shear stress. The model (21) ensures elastic ranges in all slip systems. The inelastic deformation is forced by overstresses in the slip systems. For a physical and experimental motivation of overstress models see, e.g., Krempl (1995, 1996). The viscoplastic flow rule (21) combines the assumption of elastic ranges and a rate-dependent inelastic flow which is typical for copper. In order to avoid an interference of different physical mechanisms, hardening effects are neglected in the present paper. Therefore, the critical resolved shear stresses τ_α^C and the drag stresses τ_α^D are constant during deformation. The material functions and parameters are presented in Tables 6 and 7.

3. Numerical results

3.1. Kinematics of simple and pure shear

The simulation of the free-end or fixed-end torsion generally implies the solution of boundary value problems. But the modes of pure and simple shear approximate the deformations which occur locally in free-end and fixed-end torsion experiments of a thin-walled specimen. In the present work the free-end torsion experiment is approximated by pure shear stress conditions with the shear component of the velocity gradient prescribed by $L_{12} = \dot{K} = \text{const}$. Based on this assumption the modeling of the Swift effect is reduced to a constitutive problem. The axial effects observed in experiments are assumed to be caused by the local texture development.

As a result of the aforementioned assumptions, the predictions of the polycrystal and the phenomenological model are restricted to comparisons with torsion experiments of thin-walled tubes. The stress state in solid bars differs from the pure shear state described above and the lengthening is much more pronounced in the case of thin-walled specimen compared to solid bars.

Table 6
Material functions on the microscale

Elastic law	$\tau_e = \mathbb{C}_e[\mathbf{E}_e^A]$ $\mathbb{C}_e = \mathbf{F}_e * \tilde{\mathbb{C}}$	(3)
Stiffness tensor	$\tilde{\mathbb{C}} = 3K\mathbb{P}_1^I + 2G\mathbb{P}_2^I + \zeta \frac{\sqrt{30}}{30} \left(\mathbf{I} \otimes \mathbf{I} + 2\mathbb{I} - 5 \sum_{i=1}^3 \tilde{\mathbf{g}}_i \otimes \tilde{\mathbf{g}}_i \otimes \tilde{\mathbf{g}}_i \otimes \tilde{\mathbf{g}}_i \right)$	(17)
Flow rule	$\dot{\mathbf{F}}_p \mathbf{F}_p^{-1} = \sum_\alpha \dot{\gamma}_\alpha \tilde{\mathbf{d}}_\alpha \otimes \tilde{\mathbf{n}}^\alpha$	(20)
Kinetic equation	$\dot{\gamma}_\alpha = \dot{\gamma}_0 \text{sign}(\tau_\alpha) \left(\frac{ \tau_\alpha - \tau_\alpha^C}{\tau_\alpha^D} \right)^{\frac{1}{m}}$	(21)

Table 7
Material parameters on the microscale

K	G	ζ	$\dot{\gamma}_0$	τ_α^D	τ_α^C	m
136.93 GPa	54.56 GPa	114.14 GPa	0.001 s ⁻¹	4 MPa	12 MPa	0.0125

The shear direction is denoted by \mathbf{e}_1 and the shear plane normal by \mathbf{e}_2 . The base vector \mathbf{e}_3 represents the mirror plane normal. A simple shear deformation is defined kinematically by the deformation gradient $\mathbf{F} = \mathbf{I} + K\mathbf{e}_1 \otimes \mathbf{e}_2$. The scalar $K = F_{12}$ is called shear number. A pure shear stress deformation is defined dynamically and is specified by the Cauchy stress tensor $\mathbf{T} = \tau(\mathbf{e}_1 \otimes \mathbf{e}_2 + \mathbf{e}_2 \otimes \mathbf{e}_1)$. Note that in the pure shear mode generally all diagonal components of the deformation gradient are different from one.

In torsion tests with cylindrical specimen the shear number is given by $K = RD$, where R denotes the radius of the material point and D the twist. The twist can be determined by $D = \Phi/Z$ where Z is the initial z coordinate of the cross section and Φ the respective angle of torsion. The shear direction \mathbf{e}_1 represents the tangent of the circumference of the cylinder whereas the shear plane normal \mathbf{e}_2 is aligned with the longitudinal axis of the specimen. The mirror plane normal \mathbf{e}_3 is equal to the outer normal of the cylinder. With the aforementioned settings, the axial elongation of the cylinder corresponds to a growth of the F_{22} component of the deformation gradient.

In a strain driven algorithm the shear stress is caused by the prescribed shear number K . The other components of the deformation gradient have to be chosen such that the Cauchy stress tensor has the aforementioned form. In order to find these components of the deformation gradient in each time increment a Newton procedure is applied. The components of the velocity gradient are specified such that the constraints upon the stress components are fulfilled. Then the velocity gradient is integrated over the increment by an exponential map. This approach is applied to both the phenomenological model and the Taylor–Lin model.

3.2. Monotonic Swift effect

In Fig. 1 the monotonic Swift effect is shown as it is predicted by different values of η that appears in Eq. (9) of the phenomenological model. For $\eta = 0$ there is almost no axial strain. For $\eta = 0.95$ there are two stages. The first shows a decreasing slope

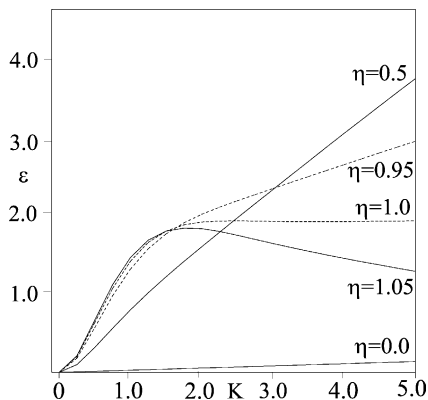


Fig. 1. Monotonic Swift effect: percentages extension ϵ vs. shear number K for different values of η (phenomenological model).

of the axial strain curve. The second shows a linear growth of the axial strain, which corresponds to measurements by Toth et al. (1992). For $\eta = 1$ the axial strains saturate as it can also be observed in experiments (Grewe and Kappler, 1964; Witzel, 1981). For $\eta = 1.05$ the axial strain decreases after passing a maximum. This behavior has also been observed (Stüwe and Turck, 1964).

3.3. Cyclic Swift effect

In Fig. 2 the predictions of the phenomenological model for polycrystalline copper are shown together with experimental data published by Swift (1947). Swift labeled the curves describing the response of the copper specimen H25 and H37. For the test H25 the shear number is increased from 0.0 to 1.3 and then decreased to -3.0 . The corresponding equivalent strain ϕ is equal to 3.29. For the test H37 the shear

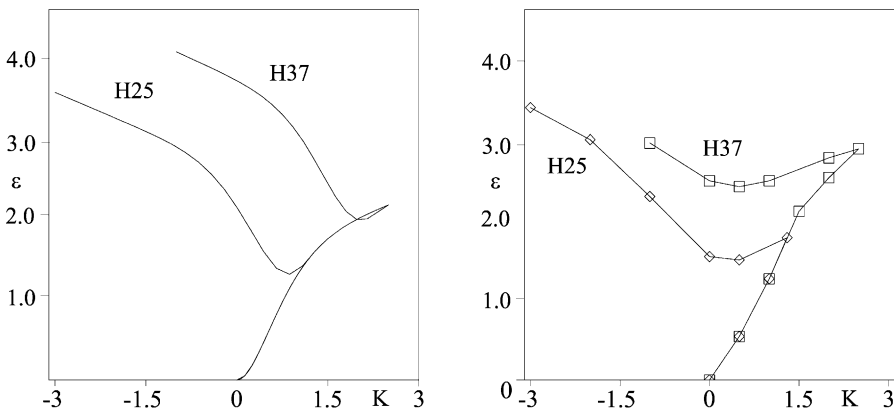


Fig. 2. Cyclic Swift effect: percentage extension ε vs. shear number K , phenomenological model with $\eta = 0.9$ (left), experimental data Swift (1947) (right).

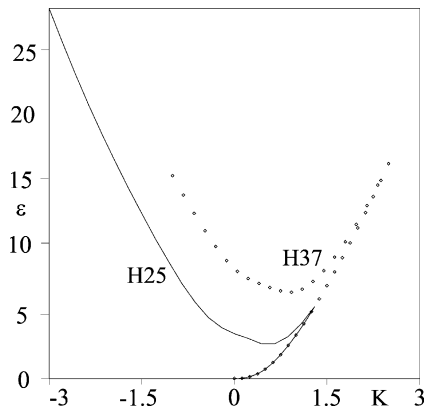


Fig. 3. Cyclic Swift effect: percentage extension ε , shear number K ; Taylor-Lin simulation with 1000 single crystals.

number is increased from 0.0 to 2.5 and then decreased to -1.0 . The corresponding equivalent strain ϕ is equal to 3.39. The phenomenological model predicts the cyclic Swift effect qualitatively. But there are quantitative differences with respect to the amount and the location of the minima of axial strain. As mentioned before Swift's data are based on solid bar experiments whereas thin-walled tubes are considered here. In Fig. 3 the predictions of the Taylor–Lin model are given which overestimate the axial elongation as already mentioned by Harren et al. (1989).

In Fig. 4 the norm of the tensor \mathbb{A}' is shown for reversed torsion tests with a shear number range equal to the aforementioned experiments H25 and H37. The anisotropy in terms of the norm $\|\mathbb{A}'\|$ saturates for a shear number equal to 2. If the torsion is reversed then the anisotropy decreases but is not reversible. The minimum of $\|\mathbb{A}'\|$ is the same for both deformation paths. Before the shear number becomes zero

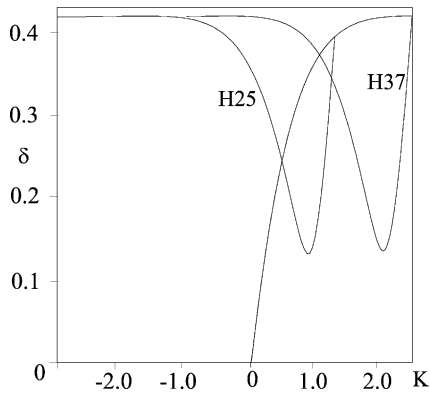


Fig. 4. Cyclic Swift effect: $\delta = \|\mathbb{A}'_E\|$ ($\mathbb{A}'_E = \tilde{\mathbf{F}} * \tilde{\mathbb{A}}'$ vs. shear number with $\eta = 0.9$ (phenomenological model).

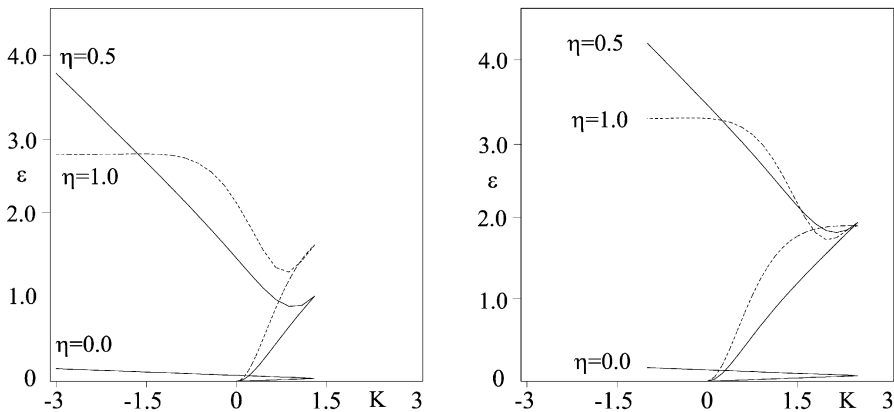


Fig. 5. Cyclic Swift effect: percentage extension ε vs. shear number K predicted by the phenomenological model for different values of η (left: H25, right: H37).

the anisotropy increases again and saturates at the same order of magnitude as for the forward torsion.

In Fig. 5 the cyclic Swift effect is shown as it is predicted by different values of η and the deformation paths H25 and H37. For $\eta=0$ there is almost no axial strain. For $\eta=0.5$ there is a linear growth of the axial strain for large shear numbers for both shear directions. For $\eta=1$ the axial strains saturate in both shear directions.

4. Conclusions

The phenomenological model for the induced elastic anisotropy has been applied to estimate the plastic anisotropy of the polycrystal. The anisotropic portion of the elasticity tensor is used to formulate an anisotropic norm in terms of the stress deviator, which specifies the flow rule. This ansatz is motivated by experimental and theoretical findings which show that the elastic and plastic anisotropy are correlated. It has been shown that the model predicts the monotonic and cyclic Swift effect. The phenomenological model reproduced the cyclic Swift effect qualitatively. In contrast to other phenomenological models suggested in the literature the present model predicts the axial effect even if the initial state of the material is isotropic.

References

- Armstrong, P., Frederick, C., 1966. A Mathematical Representation of the Multiaxial Bauschinger effect. Report RD/B/N 731.
- Barlat, F., J.M., F. D., Gracio, J., Lopes, A., Rauch, E. Plastic flow for non-monotonic loading conditions of an aluminum alloy sheet sample. *Int. J. Plasticity* (in press).
- Bertram, A., 1992. Description of finite inelastic deformations. In: Benallal, A., Billardon, R., Marquis, D. (Eds.), *Proceedings of MECAMAT'92, International Seminar on Multiaxial Plasticity*.
- Bertram, A., 1999. An alternative approach to finite plasticity based on material isomorphisms. *Int. J. Plast.* 15 (3), 353–374.
- Billington, E., 1976. Non-linear mechanical response of various metals: II permanent length changes in twisted tubes. *J. Phys.* D10, 533–552.
- Böhlke, T., 2001. *Crystallographic Texture Evolution and Elastic Anisotropy: Simulation, Modeling, and Applications*. Shaker Verlag, Dissertation, Otto-von-Guericke-Universität Magdeburg.
- Böhlke, T., Bertram, A., 1998. Simulation of texture development and induced anisotropy of polycrystals. In: Atluri, S., O'Donoghue, P. (Eds.), *Proceedings of ICES'98, Modelling and Simulation Based Engineering*.
- Böhlke, T., Bertram, A., 2000. A minimum problem defining effective isotropic elastic properties. *Z. Angew. Math. Mech.* 80 (S2), S419–S420.
- Böhlke, T., Bertram, A., 2001b. The evolution of Hooke's law due to texture development in polycrystals. *Int. J. Sol. Struct.* 38 (52), 9437–9459.
- Böhlke, T., Bertram, A., 2002. Crystallographic texture induced anisotropy in copper: an approach based on a tensorial fourier expansion of the codf. In: *Proceedings of the 6th European Mechanics of Materials Conference (EMMC6)*, pp. 273–280 (to appear in *Journal de Physique IV*).
- Bunge, H.-J., Roberts, W., 1969. Orientation distribution, elastic and plastic anisotropy in stabilized steel sheet. *J. Appl. Cryst.* 2, 116–128.
- Cho, H., Dafalias, Y., 1996. Distortional and orientational hardening at large viscoplastic deformations. *Int. J. Plast.* 12 (7), 903–925.

- Davies, G., Goodwill, D., Kallend, J., 1972. Elastic and plastic anisotropy in sheets of cubic metals. *Met. Trans.* 3, 1627–1631.
- Gil-Sevillano, J., Van Houtte, P., Aernoudt, E., 1975. Deutung der Schertexturen mit Hilfe der Taylor-Analyse. *Z. Metallkunde* 66, 367.
- Grewe, H., Kappler, E., 1964. Über die Ermittlung der Verfestigungskurve durch den Torsionsversuch und zylindrischen Vollstäben und das Verhalten von vielkristallinem Kupfer bei sehr hoher plastischer Schubverformung. *Phys. Stat. Sol.* 6, 339–354.
- Hahne, M., 1993. Beschreibung der plastischen Längsdehnung bei Torsion mit einem makroskopischen Stoffgesetz. In: *Braunschweiger Schriften zur Mechanik* Nr. 12-1993. Institut für Allgemeine Mechanik und Festigkeitslehre, TU Braunschweig.
- Harren, S., Lowe, T., Asaro, R., Needleman, A., 1989. Analysis of large-strain shear in rate-dependent face-centered cubic polycrystals: correlation of micro- and macro-mechanics. *Phil. Trans. R. Soc. Lond. A* A328, 443–500.
- Hill, R., 1948. A theory of yielding and plastic flow of anisotropic materials. *Proc. Phys. Soc. Lond. A* 193, 281–297.
- Ishikawa, H., 1999. Constitutive model of plasticity in finite deformation. *Int. J. Plasticity* 15, 299–317.
- Kallend, J., Davies, G., 1971. The elastic and plastic anisotropy of cold-rolled sheets of copper, gilding metal, and α -brass. *J. Inst. Met.* 5, 257–260.
- Krempf, E., 1994. Deformation Induced Anisotropy. RPI-Report MML 94-93.
- Krempf, E., 1995. The overstress dependence of inelastic rate of deformation inferred from transition tests. *Mat. Sci. Res. Int.* 1 (1), 3–10.
- Krempf, E., 1996. A small-strain viscoplasticity theory based on overstress. In: *Unified Constitutive laws of plastic deformation*. Academic Press Inc..
- Kuroda, M., 1997. Interpretation of the behavior of metals under large plastic shear deformations: a macroscopic approach. *Int. J. Plasticity* 13 (4), 359–383.
- Kuroda, M., 1999. Interpretation of the behavior of metals under large plastic shear deformations: comparison of macroscopic predictions to physically based predictions. *Int. J. Plast.* 15 (4), 1217–1236.
- Lin, T., 1957. Analysis of elastic and plastic strains of a face-centered cubic crystal. *J. Mech. Phys. Solids* 5, 143–149.
- Majors, P., Krempf, E., 1994. Comments on induced anisotropy, the Swift effect, and finite deformation inelasticity. *Mech. Res. Comm.* 21, 465–472.
- Man, C.-S., 1995. On the correlation of elastic and plastic anisotropy in sheet metals. *J. Elast.* 39, 165–173.
- Man, C.-S., 1998. On the constitutive equations of some weakly-textured materials. *Arch. Rat. Mech. Anal.* 143, 77–103.
- Man, C.-S., 2002. On the r -value of textured sheet metals. *Int. J. Plasticity* 18 (12), 1683–1706.
- Méric, L. and Cailletaud, G., 1992. Finite element implementation of a model for single crystals at finite strain. In: Ladevèze, P. and Zienkiewicz, O.(Eds.), *New Advances in Computational Structural Mechanics*.
- Méric, L., Cailletaud, G., Gaspérini, M., 1994. Calculations of copper bicrystal specimens submitted to tension–compression tests. *Acta Metall. Mater.* 42 (3), 921–935.
- Miller, M., McDowell, D., 1996. Modeling large strain multiaxial effects in fcc polycrystals. *Int. J. Plast.* 12 (7), 875–902.
- Montheillet, F., Cohen, M., Jonas, J., 1984. Axial stresses and texture development during the torsion testing of Al, Cu and α -Fe. *Acta Metall.* 32 (11), 2077–2089.
- Montheillet, F., Gilormini, P., Jonas, J., 1985. Relation between axial stresses and texture development during torsion testing: a simplified theory. *Acta Metall.* 33 (4), 705–717.
- Pan, W.-F., 1996. Endochronic analysis for finite elasto-plastic deformation and application to metal tube under torsion and metal rectangular block under biaxial compression. *Int. J. Plasticity* 12 (10), 1287–1316.
- Pan, W.-F., 1997. Endochronic simulation for finite visco-plastic deformation. *Int. J. Plasticity* 13 (6-7), 571–586.
- Portier, L., ad Calloch, S., Marquis, D., Geyer, P., 2000. Ratchetting under tension-torsion loadings: experiments and modelling. *Int. J. Plasticity* 16, 303–335.

- Stickels, C., Mould, P., 1970. The use of Young's modulus for predicting the plastic-strain ratio of low-carbon steel sheets. *Met. Trans.* 1, 1303–1312.
- Stüwe, H., Turck, H., 1964. Zur Messung von Fließortkurven im Torsionsversuch. *Z. Metallk.* 55, 699–703.
- Swift, H., 1947. Length changes in metals under torsional overstrain. *Engineering* 163, 253–257.
- Taylor, G., 1938. Plastic strain in metals. *J. Inst. Metals* 62, 307–324.
- Toth, L., Jonas, J., Daniel, D., Bailey, J., 1992. Texture development and length changes in copper bars subjected to free end torsion. *Textures Microstruct.* 10, 245–262.
- Van der Giessen, E., Wu, P., Neale, K., 1992. On the effect of plastic spin on large strain elastic-plastic torsion of solid bars. *Int. J. Plast.* 8, 773–801.
- von Mises, R., 1928. Mechanik der plastischen Formänderung bei Kristallen. *Z. Angew. Math. Mech.* 8 (3), 161–185.
- Witzel, W., 1981. Längenänderungen und Längskräfte bei Torsionsbeanspruchung. In: Stüwe, H.-P. (Ed.), *Verformung und Bruch*, Verlag der Österreichischen Akademie der Wissenschaften.
- Wu, H.-C., 2003. On finite plastic deformation of anisotropic metallic materials. *Int. J. Plasticity* 19 (1), 91–119.
- Wu, H.-C., Xu, Z., Wang, P., 1997. Torsion test of aluminum in the large strain range. *Int. J. Plasticity* 13 (10), 873–892.
- Xiao, H., Bruhns, O., Meyers, A., 2001. Large strain responses of elastic-perfect plasticity and kinematic hardening plasticity with the logarithmic rate: Swift effect in torsion. *Int. J. Plasticity* 17, 211–235.
- Zbib, H., 1991. On the mechanics of large deformations: noncoaxiality, axial effects in torsion and localization. *Acta Mech.* 87, 179.
- Zbib, H., Aifantis, E., 1998. On the concept of relative and plastic spin and its implications to large deformation theories. Part I: hypoelasticity and vertex-type plasticity. *Acta Mech.* 75, 15.